Probing Lorentz violation in neutrino propagation from a core-collapse supernova

John Ellis,[1,2] Hans-Thomas Janka,[3] Nikolaos E. Mavromatos,[1,2] Alexander S. Sakharov,[2,4] and Edward K. G. Sarkisyan[2,5]

[1]*Theoretical Particle Physics and Cosmology Group, Department of Physics, King's College London,*
Strand, London WC2R 2LS, United Kingdom
[2]*Physics Department, CERN, CH-1211 Geneva 23, Switzerland*
[3]*Max-Planck-Institut für Astrophysik, Karl-Schwarzschild-Str. 1, D-85748 Garching, Germany*
[4]*Department of Physics, Wayne State University, Detroit, Michigan 48202,USA*
[5]*Department of Physics, University of Texas at Arlington, Arlington, Texas 76019, USA*

Supernova explosions provide the most sensitive probes of neutrino propagation, such as the possibility that neutrino velocities might be affected by the foamy structure of space-time thought to be generated by quantum-gravitational effects. Recent two-dimensional simulations of the neutrino emissions from core-collapse supernovae suggest that they might exhibit variations in time on the scale of a few milliseconds. We analyze simulations of such neutrino emissions using a wavelet technique, and consider the limits that might be set on a linear or quadratic violation of Lorentz invariance in the group velocities of neutrinos of different energies, $v/c = [1 \pm (E/M_{\nu LV1})]$ or $[1 \pm (E/M_{\nu LV2})^2]$, if variations on such short time scales were to be observed, where the mass scales $M_{\nu LVi}$ might appear in models of quantum gravity. We find prospective sensitivities to $M_{\nu LV1} \sim 2 \times 10^{13}$ GeV and $M_{\nu LV2} \sim 10^6$ GeV at the 95% confidence level, up to 2 orders of magnitude beyond estimates made using previous one-dimensional simulations of core-collapse supernovae. We also analyze the prospective sensitivities to scenarios in which the propagation times of neutrinos of fixed energies are subject to stochastic fluctuations.

I. INTRODUCTION

Supernovae provide some of the most sensitive probes of neutrino physics [1], as exemplified by studies of the neutrinos detected after emission from SN 1987a [2]. Excellent prospects for improving these studies would be offered by a future galactic core-collapse supernova. Crucial inputs into estimates of the prospective sensitivities of such studies are provided by supernova simulations. In the past, these simulations have mainly been one-dimensional, i.e., implicitly assuming that the collapse is spherically symmetric. Clearly, more realistic simulations are desirable, and more recently two-dimensional hydrodynamic models, i.e., implicitly assuming only cylindrical symmetry, have become available, in which multigroup, three-flavor neutrino transport has been treated by different (relatively sophisticated) approximations [3–5]. These have revealed several interesting features, the most relevant for our analysis being the appearance of fast time variations in the neutrino emission [4,5], as seen in the top panel of Fig. 1. It was shown that these could be observable in the IceCube experiment [6], and could exhibit a quasi-periodicity of $\mathcal{O}(10)$ ms, similar to the natural time scale of reverberations associated with hydrodynamic instabilities in the supernova core. It is desirable to confirm the predicted appearance of such features in neutrino emissions from core-collapse supernovae through more detailed simulations, in particular, in three dimensions.[1]

---
[1]For first steps in this direction, see [7,8].

Nevertheless, we find these features sufficiently interesting and well motivated to consider the sensitivity to effects in neutrino propagation that would become available if such rapid time variations were in fact to be observed.

The most obvious such effect is that of neutrino mass. Nonzero masses cause neutrinos to travel at less than the speed of light, by an amount that *decreases* with increasing neutrino energy. This causes any time structure that appears simultaneously in emissions over a range of energies to spread out before arrival at the Earth, an effect that was exploited to set an upper limit on neutrino masses using data from SN 1987a [9]. Though an interesting demonstration of principle, that limit was not competitive with laboratory and cosmological limits, and even the increase in sensitivity suggested by the more recent two-dimensional simulations seems unlikely to be competitive.

Another possibility is to use the neutrino emissions from core-collapse supernovae to constrain effects on neutrino propagation such as might be induced by "foamy" quantum-gravitational fluctuations in the fabric of space-time [10]. Such space-time foam effects could include a refractive index (i.e., a change in the neutrino or photon velocity that depends on energy) [11–15], dispersion in propagation at fixed energy [16], and a loss of coherence [17]. Models suggest that any such effects should *increase* with increasing neutrino energy E, being proportional, e.g., to $E/M_{\nu LV1}$ or $(E/M_{\nu LV2})^2$, where the mass scales $M_{\nu LVi}$ might originate from quantum gravity. As such, they would be easily distinguishable, in principle, from the effect on neutrino propagation of a neutrino mass. Estimates have been given [15] of the possible sensitivity to such effects
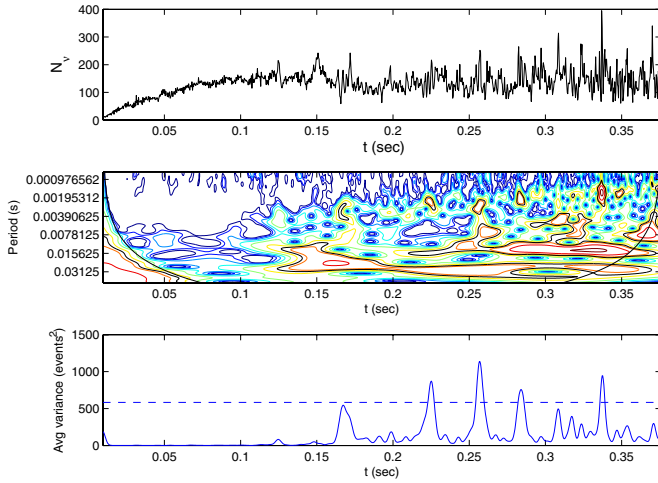
FIG. 1 (color online). *Top panel*: The time series of the neutrino emission from the two-dimensional simulation of a core-collapse supernova found in [5]. The time profile is sampled in $1024(2^{10})$ bins. *Middle panel*: The local wavelet power spectrum of the neutrino emission time series, obtained using the Morlet wavelet function (12) normalized by $1/\sigma^2$. The vertical axis is the Fourier period (in seconds), and the horizontal axis is the time of the neutrino emission. The red contours enclose regions that differ from white noise at greater than the 95% confidence level. The cone of influence, where edge effects become important, is indicated by the concave solid lines at the edges of the support of the signal. Comparing the width of a peak in the wavelet power spectrum with this decorrelation time, one can distinguish between a spike in the data (possibly due to random noise) and a harmonic component at the equivalent Fourier frequency. *Bottom panel*: The average power in the 0.002–0.003 s band. The dashed line is the 95% confidence level obtained from (28).

that could be provided by a core-collapse supernova explosion in our Galaxy, e.g., sensitivity to $M_{\nu\mathrm{LV}1} \sim 2 \times 10^{11}$ GeV or $M_{\nu\mathrm{LV}2} \sim 2 \times 10^5$ GeV for a refractive index >1, corresponding to increasingly subluminal propagation of energetic neutrinos. These prospective sensitivities are considerably greater than those offered by terrestrial long-baseline neutrino experiments [18]: the latters' beams have much finer time structures, but they are handicapped by their much shorter propagation distances.

The estimates above were based on the earlier simulations of the core collapse of a supernova that yielded emissions over a period of seconds without any finer time structure. A priori, the observation of time structures on the scale of $\mathcal{O}(10)$ ms in the neutrino emissions from core-collapse supernovae, as suggested by more recent two-dimensional simulations [4,5], would provide the possibility to constrain foamy effects on neutrino propagation a couple of orders of magnitude more sensitively than was previously estimated. In this paper, we use such a simulation to estimate the prospective sensitivity to a neutrino refractive index and dispersion in propagation at fixed energy, applying a wavelet analysis to the simulated neutrino signals published in [5].

We find that the prospective sensitivities to novel effects in neutrino propagation would indeed be enhanced by 2 orders of magnitude if the neutrino signals from core-collapse supernovae do exhibit the fine-scale time structures suggested by two-dimensional simulations. In the first instance, these sensitivities may be expressed for energy-dependent time shifts τ_l or dispersions at fixed energy, both expressible in units of s/MeV^l for effects $\propto E^l$. Knowing the distance from any given supernova, these sensitivities may be translated into sensitivities to model parameters such as the $M_{\nu\mathrm{LV}l}$ introduced above. Hypothesizing a typical distance of 10 kpc we find, for example, sensitivities to $M_{\nu\mathrm{LV}1} \sim 2 \times 10^{13}$ GeV and $M_{\nu\mathrm{LV}2} \sim 10^6$ GeV at the 95% confidence level. We emphasize these sensitivities could immediately become *lower* limits if time structures are observed. The absence of such time structures could provide *upper* limits if the predictions by two-dimensional simulations of short time structures could be validated, assuming that no astrophysical effect during propagation could wash out the effect.

This subject has become much more topical during the finalization of this paper, with the publication of an analysis of OPERA data [19] using a technique similar to that developed in [15]. This reports possible superluminal neutrino propagation with velocity exceeding that of light, c, by an amount δv: $\delta v/c \sim 2.5 \times 10^{-5}$, corresponding to $M_{\nu\mathrm{LV}1} \sim 1.1 \times 10^6$ GeV or $M_{\nu\mathrm{LV}2} \sim 5.6 \times 10^3$ GeV [20], smaller than the lower limits established in [15] using SN1987a data. Thus, a simple power law fit jointly to the SN1987a data and OPERA δv would probably require an energy dependence steeper than E^2, in apparent conflict with the energy spectrum of the neutrino events measured by OPERA. The superluminal neutrino interpretation of the OPERA data is subject to many other experimental and phenomenological constraints, and one should not assume that it will survive further scrutiny. Nevertheless, this episode heightens awareness of the importance of probing fundamental principles such as the universality of the velocity of light as sensitively as possible, and our analysis based on two-dimensional simulations of supernova explosions shows that they could provide unparalleled sensitivity to novel effects in neutrino propagation.

II. INGREDIENTS IN THE ANALYSIS

A. Quantum-gravity models for non-standard neutrino propagation

As mentioned in the Introduction, various possibilities for nonstandard neutrino propagation are suggested by phenomenological models based on approaches to quantum gravity [15,17]. This is because such models entail microscopic fluctuations of space-time, due to curvature fluctuations and/or, in certain theories, space-time defects. Specifically, in brane theories based on string theory [14], the latter may be modeled as pointlike structures that cross the brane Universe from the bulk, giving space-time a

foamy nature at microscopic scales. In our current state of knowledge of string theory, the string scale is essentially a free parameter to be constrained by low-energy phenomenology, and, in particular, by constraints on nonstandard neutrino propagation.

1. Modified dispersion relation

One of the most explored avenues for experimental probes of (some models of) space-time foam is to search for Lorentz violation induced in the propagation of matter particles by their interactions with this foamy space-time medium. In certain string-inspired models of foam, the presence of a medium affects the dispersion relations of certain species of matter particles [14,16]. In the simplest formulation of the effects of the foam, in a first approximation only electrically neutral particles interact with the medium, so that photons and neutrinos are the most sensitive probes of such models. In these models, the modification of a particle's dispersion relation is a consequence of the microscopic Lorentz violation induced by the recoil of a space-time defect during its nontrivial interaction with the open-string state that represents the particle excitation in a brane Universe [14,16]. In the case of photon propagation, this effect is manifested as a vacuum refractive index. For purely string-theoretical reasons, the induced refractive index is *subluminal*, implying that, if a beam of photons with different energies is emitted simultaneously from a source, the arrival times of more energetic photons will be delayed compared to their lower-energy counterparts.[2]

In the case of neutrinos, regarded as (almost) massless particles, a similar effect might be expected, namely, a delayed arrival of the more energetic neutrinos from cosmic sources, assuming that the neutrinos of different energies are emitted (almost) simultaneously. One may therefore consider foam-induced Lorentz violation that is expressed via a neutrino group velocity, v_g, that may depend either linearly or quadratically on the energy of the neutrino:

$$v_g/c = 1 \pm (E/M_{\nu \mathrm{LV}l})^l, \qquad l = 1 \quad \text{or } 2. \quad (1)$$

As discussed in [15], lower limits on $M_{\nu \mathrm{LV}l}$ may be obtained by requiring that narrow peaks in neutrino emission over a range of energies not be broadened significantly, or even washed out, and this is the strategy advocated here using emissions from a supernova.

2. Dispersion of a wave packet

A second effect that may also be induced by quantum-gravity foam models is a spread in the width of the wave packet, which may depend on the neutrino energy. This could arise from an energy-dependent neutrino velocity of

the type discussed above, or from a stochastic spread in neutrino velocities at fixed energy [16].

Consider, for example, a neutrino wave packet that is Gaussian in the "approximately" light-cone variable $x - v_g t$, where the group velocity $v_g = d\omega/d\kappa$ is near the speed of light for the relativistic, almost massless neutrinos that we consider here, allowing for a generic dispersion relation $\omega = \omega(\kappa)$ with $\kappa \equiv |\vec{\kappa}|$ being the spatial momentum amplitude. For neutrinos that are almost massless, the analysis is similar to that given in [16]. The square of the neutrino amplitude is given in general by

$$|f(x, t)|^2 = \frac{A^2}{\sqrt{1 + \frac{\alpha^2 t^2}{(\Delta x_0)^4}}} \exp\left\{-\frac{(x - v_g t)^2}{2(\Delta x_0)^2 [1 + \frac{\alpha^2 t^2}{(\Delta x_0)^4}]}\right\}, \quad (2)$$

where $|\Delta x_0|$ is the spread at $t = 0$, $\alpha = \frac{1}{2}(d^2\omega/d^2\kappa)$, and we assume that the neutrino wave packet has a Gaussian distribution in the approximately light-cone variable $x - v_g t$.

We see immediately in (2) that the quadratic term α in the dispersion relation does not affect the motion of the peak, but only the spread of the Gaussian wave packet:

$$|\Delta x| = \Delta x_0 \sqrt{1 + \frac{\alpha^2 t^2}{(\Delta x_0)^4}}, \quad (3)$$

which therefore increases with time. The quadratic term α also affects the peak amplitude of the wave packet: the latter decreases as the spread (3) increases, in such a way that the integral of $|f(x, t)|^2$ is constant.

If the neutrinos were exactly massless, then, as in the case of photons, the quantity α would receive nonzero contributions only from anomalous terms in the dispersion relation due to quantum gravity of the form (1) [16]. In the linear case, $l = 1$, such corrections would be independent of the energy of the neutrino. In the presence of small neutrino masses, $m \ll \kappa$, there are always contributions to α from terms of the form

$$\alpha = \frac{m^2}{\kappa^3}, \qquad m \ll \kappa. \quad (4)$$

Such terms contribute to the spread of the wave packet, but decrease with the neutrino momentum, in contrast to quantum-gravity effects that are expected to be constant or to increase as functions of the neutrino energy (momentum), depending whether the energy dependence of the refractive index is linear or quadratic.

Hence, we may parametrize the spread α generically as in (3), with the parameter α having a power-law dependence on the neutrino momentum κ:

$$\alpha = \frac{m^2}{\kappa^3} - l(l + 1) \frac{\kappa^{l-1}}{M_{\nu \mathrm{LV}l}^l}, \quad (5)$$

with $l = 1$ or 2, where the stochastic case is denoted by the tilde in the suffix of the quantum-gravity scale. To leading

---

[2]As a bonus, this avoids any constraints due to the emission of Čerenkov radiation by energetic photons [21].

order in the small neutrino mass, we may replace k by the (average) neutrino energy E of the wave packet. This effect leads to a potentially independent way of detecting space-time foam [10], although we find that it is not competitive with limits coming directly from time-of-flight measurements, as discussed below.

3. Wave-packet spread induced by stochastic fluctuations in neutrino velocities

Another phenomenon that may also be induced by quantum-gravity foam models is stochastic fluctuation in the velocities of different neutrinos with the same energy [16]. As an example how this type of effect might arise from space-time foam, we consider the possibility of light-cone fluctuations.

In the string-inspired models of space-time foam that we consider here, these may be induced by the summation over world-sheet surfaces with higher-genus topologies. These result in an effective stochastic fluctuation of the light-cone of order [16]

$$\delta c \sim 8 g_s^2 \frac{E}{M_s c^2},\qquad(6)$$

where M_s is the string scale, g_s is the string coupling, and E is the average energy of the massless (or, in the case of the neutrino, almost massless) probe.

Light-cone fluctuations of the form (6) would also lead to a spread in the Gaussian wave packet, which is distinct from the spread induced by the refractive index (3). The spread induced by light-cone fluctuations would be linear in the quantum-gravity scale, as seen from (6). Such an effect would lead to a stochastic spread in the arrival times of photons or neutrinos of order

$$\delta \Delta t = \frac{L}{c\Lambda} E,\qquad \Lambda \equiv \frac{M_s c^2}{8 g_s^2},\qquad(7)$$

where L is the distance of the observer from the source.[3] We emphasize that, in contrast to the variation (1) in the refractive index—which refers to photons of different energies—the fluctuation (7) characterizes the statistical spread in the velocities of particles *of the same energy*. We note that the stochastic effect (7) is suppressed compared to the linear ($n = 1$) refractive index effect (1) by an extra power of the string coupling g_s (we recall that, in the string model, $M_{\nu LV1} \propto M_s/g_s$).

The light-cone fluctuation effects may be thought of as inducing a time-independent spread σ in a neutrino wave packet that can be parametrized as (see later)

$$\mathcal{P}(t) \sim e^{-((t-t_0)^2/2\sigma^2)},\qquad(8)$$

---

[3] In our analysis below, we may ignore effects associated with the expansion of the Universe, as we are dealing with neutrinos from galactic supernovae.

where

$$\sigma^2 = \sigma_0^2 + c_1^2 \frac{E^l}{\underset{\nu LVl}{\underbrace{M^l}}},\qquad l = 0 \quad \text{or } 1.\qquad(9)$$

The expression (8) is distinct from the relativistic Gaussian wave packet used above and in [16]. In the latter case, the stochastic light-cone fluctuations already affect the spread (3) $|\Delta x_0|^2$ at $t = 0$, which then may be identified with the σ^2 in (9).

B. Two-dimensional simulation of a core-collapse supernova

The analysis presented in this paper is based on the results of a two-dimensional, i.e., axisymmetric, core-collapse simulation for a $15 M_\odot$ star computed with the high-density equation of state of Lattimer and Swesty [22]. The properties of the neutrino signal calculated in this model were discussed in detail in [5].

Unlike one-dimensional, i.e., spherically symmetric, models, the neutrino emission during the post-bounce accretion phase exhibits rapid time variability because of anisotropic mass flows in the accretion layer around the newly formed neutron star. These flows are a consequence of convective overturn as well as the standing accretion-shock instability (SASI; [23]), which lead to large-scale, nonradial mass motions in the layer between the protoneutron star surface and the accretion shock. Locally enhanced mass infall to the compact remnant and asymmetric compression create hot spots that can produce transiently neutrino radiation that is more luminous and with a harder spectrum, emitted in preferred directions. Temporal variations of the luminosities and mean energies are expected to persist during the whole accretion phase, which can last hundreds of milliseconds. For electron neutrinos and antineutrinos, such variations could yield fractional changes of 10% and even higher during the most violent phases of core activity in two-dimensional models with no or only slow rotation [4,5]. The corresponding effects are somewhat damped for muon and tau neutrinos, because a smaller fraction of these neutrinos is produced in the outer layers of the protoneutron star where asymmetric accretion causes the largest perturbations.

The fluctuating neutrino emission has been shown to trigger a clearly detectable signature in the response of the IceCube detector in the case of a neutrino burst from a future Galactic supernova. Peaks of the power spectrum of the event rate are expected at the typical frequencies of the SASI and convective activity (between several tens of Hz and roughly 200 Hz) [5].

While a softer nuclear equation of state (allowing for a more compact protoneutron star) seems to favor larger signal amplitudes [5], several other sources of uncertainty in the model predictions need to be mentioned. One concerns the neutrino transport description that is used, which

even in the most sophisticated current multidimensional (two- or three-dimensional) models cannot be handled without approximations. In Ref. [5], neutrino predictions were obtained in a scheme in which the full energy dependence of the transport problem was accounted for (including Döppler shifting, gravitational redshifting, and neutrino redistribution in energy space by scattering reactions) but the two dimensionality of the transport was treated in a "ray-by-ray" approximation. This means that the spatial transport was described by N spherically symmetric (radial) problems with N being the number of lateral grid zones, and it implies that the directional averaging or smoothing of the neutrino emission due to radiation received by an observer from different areas of the emitting surface is underestimated. However, in Ref. [5] also data averaged over hemispheres (northern, southern, equatorial) were considered, which still led to easily detectable signatures. Moreover, the basic effects discussed in [5] were confirmed by true multiangle two-dimensional transport results in Ref. [4], though with the limitation of not including energy-bin coupling due to the effects mentioned above. We note also that flavor oscillations between $\bar{\nu}_e$ and muon or tau antineutrinos, whose emission variations have lower amplitudes, reduces the modulations of the event rate in the IceCube detector only moderately.

The largest uncertainty in current model predictions results from the two-dimensional nature of the most detailed simulations. Three-dimensional modeling of stellar core collapse is still in its infancy, and well-resolved simulations with energy-dependent neutrino transport are currently not available. First steps in this direction were reported in Ref. [7], but the models are either not evolved for interestingly long post-bounce times or the employed numerical resolution is poor and the neutrino data are not conclusive with respect to the effects discussed here. In constrast, Ref. [8] employed a simpler, energy-averaged ("grey"), ray-by-ray neutrino transport approximation and could follow the evolution of collapsing stellar cores in three dimensions over several hundred milliseconds of post-bounce accretion, through explosion, into the subsequent neutrino cooling of the nascent neutron star. The radiated neutrino signal as visible by a distant observer was evaluated in [8] and also revealed variations with time on the scale of a few milliseconds, however with an amplitude of several percent only, instead of the 10% or more found in two-dimensional simulations.

An analysis of the detectable consequences is in progress. Whilst in a two-dimensional simulation the existence of a symmetry axis directs the SASI sloshing motions of the shock and of the accretion flows, these motions are similar in all directions in three dimensions and thus appear to develop smaller amplitude in any particular direction, leading to a reduced fractional fluctuation of the observable neutrino emission. It should be noted, however, that the existing three-dimensional models still contain severe approximations and do not explore the range of interesting possibilities. In particular, they do not include the effects of rotation in the stellar core, which even for slow rates could significantly influence the growth of SASI spiral modes [24].

We base our analysis here on the more mature two-dimensional simulations, though adopting a somewhat optimistic point of view, in that we determine the maximal effects that can be expected within the detailed two-dimensional models currently available. We therefore consider (north-) polar emission (i.e., no averaging of luminosities and spectra over a wider range of latitudes) of electron antineutrinos, as predicted by the $15 M_\odot$ simulation with the relatively soft equation of state of Lattimer and Swesty in Ref. [5]. Possible flavor conversions between electron antineutrinos and heavy-lepton antineutrinos are ignored.

C. Detector response to the time-varying SN neutrino signal

As was discussed in detail in [5], IceCube or a future megaton-class water Čerenkov detector would be very promising for detecting the time-varying neutrino signal from a future galactic SN. Such detectors are designed to detect a large number of Čerenkov photons produced by neutrino events, and a single photon produced by a given neutrino can tag its arrival time. Hence the term "event" can be used interchangeably to refer to photon or neutrino detection. In the case of a SN at the fiducial distance of 10 kpc assumed here, the photon detection rate can be as high as $\sim 10^3/\text{ms}$. This is similar to the intrinsic background rate estimated for IceCube. A megaton-scale water Čerenkov detector would achieve neutrino detection rates similar to IceCube and, in addition, would provide event-by-event information. Therefore, IceCube may serve as a benchmark detector for estimating a typical detection rate achievable for a time-varying SN neutrino signal.[4]

A schematic model of the IceCube detector response to a SN neutrino signal was used in [5] to estimate the detection rate, including efficiencies, for Čerenkov photons originating from the dominant inverse-beta reaction $\bar{\nu}_e + p \rightarrow n + e^+$:

$$R_{\bar{\nu}_e} = 114 \, \text{ms}^{-1} \frac{L_{\bar{\nu}_e}}{10^{52} \, \text{erg} \, \text{s}^{-1}} \left(\frac{10 \, \text{kpc}}{D} \right)^2 \left(\frac{E_{\text{rms}}}{15 \, \text{MeV}} \right)^2, \quad (10)$$

where $L_{\bar{\nu}_e}$ and D are the SN luminosity and distance, respectively. The definition [5]

$$E_{\text{rms}}^2 \equiv \frac{<E^3>}{<E>} \quad (11)$$

is used, where the average is to be taken over the neutrino distribution function. This estimate for the photon count

---

[4]For the Super-Kamiokande detector with fiducial volume 22.5 kt, the corresponding neutrino detection rate is approximately 2 orders of magnitude smaller, but essentially background free.
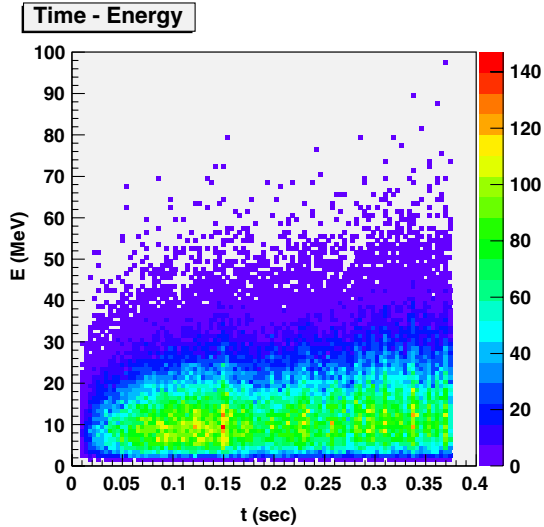
FIG. 2 (color online). The distribution of times and energies assigned to individual neutrinos in one statistical realization of the thermal spectra found in the simulation [5].

rate uses an approximate inverse-beta cross section of $\sigma = 9.52 \cdot 10^{-44}$ cm$^2(E_{\bar{\nu}_e}/\text{MeV}^2)$.

We assume in our analysis that the neutrino data collected from a supernova explosion will consist of a list of individual neutrino events with measured energies E_i and arrival times t_i, as motivated by the fact that a low-energy water Čerenkov or scintillator detector is able to register the time t_i of every event with high precision. The results of the simulation performed along the line of Sec. II B and described extensively in [5] are presented as a set of primary energy fluxes within time periods of durations $\simeq$ 3–5 ms, and each individual flux can be represented by a black-body spectrum with a given value of the mean energy. The fluxes are mapped into the photon counting rates using the benchmark detector response rate (10). Knowing the mean and total energy of neutrinos leading to the photon counting rate in each time period, we assign statistically to each event a specific time of emission and energy. The distribution of one implementation of such neutrino time-energy assignments folded with the benchmark detector response (10) is presented in Fig. 2. In order to obtain robust estimates of the sensitivities to novel effects in neutrino propagation as discussed below, we make a number of different implementations of the neutrino emission, all with independent statistical realizations of the thermal spectra. We then apply a technique based on wavelet transforms to these implementations, and analyze statistically the sensitivities to new physics that they may have.

D. Wavelet analysis technique

We use a wavelet transform technique (see [25] for a review) to analyze the neutrino time series generated by the simulated supernova explosion, as it is well adapted to capturing possible signatures of nonstationary power at many different frequencies.

Consider a time series, x_n, $n = 0, \ldots, N - 1$, in bins of equal width δt. The wavelet transform is based on a wavelet function, $\psi_0(\eta)$, that depends on a dimensionless "time" parameter η. To be admissible as a wavelet transform, this function must have zero mean and be localized in both time and frequency space. In choosing the wavelet function, there are several factors which should be considered:

Nonorthogonality: The term "wavelet function" may be applied generically to either orthogonal or nonorthogonal wavelets. In orthogonal wavelet analysis, the number of convolutions at each scale is proportional to the width of the wavelet basis at that scale. This produces a wavelet spectrum that contains discrete blocks of wavelet power, and is useful for signal processing as it gives the most compact representation of the signal. Unfortunately for time series analysis, an aperiodic shift in the time series produces a different wavelet spectrum. Conversely, a nonorthogonal analysis is highly redundant at large scales, where the wavelet spectrum at adjacent times is highly correlated. The term "wavelet basis" refers only to an orthogonal set of functions, and an orthogonal basis implies the use of the discrete wavelet transform, whereas nonorthogonal wavelet functions can be used with either discrete or continuous wavelet transforms. A nonorthogonal transform is useful for the analysis of time series where smooth, continuous variations in wavelet amplitude are expected, and is used in this study.

Complexity: A real wavelet function provides only a single component, and can be used to isolate peaks or discontinuities. On the other hand, a complex wavelet function provides information about both the amplitude and phase, and is better adapted for capturing oscillatory behavior. This is the choice made in this paper.

Width: For concreteness, the width of a wavelet function is defined as the *e*-folding "time" of the wavelet amplitude. The resolution of a wavelet function is determined by the balance between the width in real space and the width in Fourier space. A narrow (in time) function will have good time resolution but poor frequency resolution, while a broad function will have poor time resolution, but good frequency resolution.

Shape: The wavelet function should reflect the type of feature present in the time series. For time series with sharp jumps or steps, one would choose a boxcarlike function, whereas for a smoothly varying time series one would choose a smooth function such as a damped cosine. If one is primarily interested in wavelet power spectra, then the choice of wavelet function is not critical, and one function will give qualitatively similar results to another.

Among common nonorthogonal wavelet functions, the Morlet wavelet is complex and contains a number of oscillations sufficient to detect narrow features of the power

spectrum, and is the choice made here. It consists of a plane wave modulated by a Gaussian function in a variable η:

$$\psi_0(\eta) = \pi^{-1/4} e^{i\omega_0 \eta} e^{-\eta^2/2}, \qquad (12)$$

where ω_0 is a dimensionless frequency.

The continuous wavelet transform of a discrete sequence x_n is defined as the convolution of x_n with a scaled and translated version of $\psi_0(\eta)$ [5]:

$$W_n(s) = \Sigma_{n'=0}^{N-1} x_{n'} \psi^* \left[\frac{(n'-n)\delta t}{s} \right]. \qquad (13)$$

By varying the wavelet scale s and translating along the localized time index n, one can construct a picture showing both the amplitude of any features versus the scale and how this amplitude varies with time. Although it is possible to calculate the wavelet transform using (13), it is convenient and faster to perform the calculations in Fourier space.

To approximate the continuous wavelet transform, the convolution (13) should be performed N times for each scale, where N is the number of points in the time series. By choosing N points, the convolution theorem allows us to perform all N convolutions simultaneously in Fourier space using a discrete Fourier transform:

$$\hat{x}_k = \frac{1}{N} \Sigma_{n=0}^{N-1} x_n e^{-2\pi i k n / N}, \qquad (14)$$

where $k = 0, \ldots, N-1$ is the frequency index. In the continuous limit, the Fourier transform of a function $\psi(t/s)$ is given by $\hat{\psi}(s\omega)$. According to the convolution theorem, the wavelet transform is the Fourier transform of the product:

$$W_n(s) = \Sigma_{k=0}^{N-1} \hat{x}_k \psi^*(s\omega_k) e^{i\omega_k n \delta t}, \qquad (15)$$

where $\omega_k = +\frac{2\pi k}{N\delta t}$ and $-\frac{2\pi k}{N\delta t}$ for $k \leq \frac{N}{2}$ and $k > \frac{N}{2}$, respectively.

As already mentioned, following the criteria for selecting wavelets for a particular task described above, in this paper we process the neutrino signal using Morlet wavelets (12) of frequency ω_0, which takes the form

$$\hat{\psi}_0(s\omega) = \pi^{-1/4} H(\omega) e^{-(s\omega - \omega_0)^2/2} \qquad (16)$$

after the Fourier transform, where $H(\omega)$ is the Heaviside function: $H(\omega) = 1$ if $\omega > 0$, and zero otherwise. The width of this wavelet, defined as the e-folding time of the wavelet amplitude, is $\tau_s = \sqrt{2}s$. The function $\hat{\psi}_0$ is normalized to unity:

$$\int |\hat{\psi}_0(\omega')|^2 d\omega' = 1 \qquad (17)$$

and, in order to ensure that the wavelet transforms (15) at all scales s are directly comparable to each other and to the

transforms of other time series, the wavelet functions ψ_0 at other scales are normalized to have unit energy:

$$\hat{\psi}(s\omega_k) = \sqrt{\left(\frac{2\pi s}{\delta t}\right)} \hat{\psi}_0(s\omega_k). \qquad (18)$$

This implies that

$$\Sigma_{k=0}^{N-1} |\hat{\psi}(s\omega_k)| = N. \qquad (19)$$

Using the convolution formula (13), the normalization of the function ψ is

$$\psi \left[\frac{(n'-n)\delta t}{s} \right] = \sqrt{\frac{\delta t}{s}} \psi_0 \left[\frac{(n'-n)\delta t}{s} \right], \qquad (20)$$

and the wavelet power spectrum is defined by $|W_n(s)|^2$. It is desirable to find a common normalization for the wavelet spectrum. Using the normalization in (18), and referring to (15), the expectation value for $|W_n(s)|^2$ is equal to N times the expectation value for $|\hat{x}_k|^2$. For a white-noise time series, this expectation value is σ^2/N, where σ^2 is the variance. Thus, for a white-noise process, the expectation value for the wavelet transform is $|W_n(s)|^2 = \sigma^2$ for all n and s.

Once the wavelet function is chosen, it is necessary to choose a set of scales s to use in (15). For our purposes, it is convenient to choose discrete scales related by powers of two:

$$s_j = 2^{j\delta j} s_0, \quad j = 0, 1, \ldots, J, \quad J = \frac{1}{\delta j} \log_2\left(\frac{N\delta t}{s_0}\right), \qquad (21)$$

where s_0 is the smallest resolvable scale and J determines the largest scale. The choice of a sufficiently small δj depends on the width in spectral space of the wavelet function. In the case of the Morlet wavelet, $\delta j \approx 0.5$ is the largest value that still gives an adequate sampling scale. In the middle panel of Fig. 1, we use $N = 1024$, $\delta t = 1.785 \cdot 10^{-4}$ s, $s_0 = 2\delta t$, $\delta j = 0.125$, and $J = 48$. We display in this panel the "cone of influence," which is indicated by the concave solid lines at the edges of the support of the signal: this is the region of the wavelet spectrum where edge effects become important, defined as the e-folding time for the wavelet autocorrelation power at each scale, and that also gives a measure of the decorrelation time for a single spike in the time series.

Since the wavelet transform is a bandpass filter with a known response function (the wavelet function), it is possible to reconstruct the original time series using either deconvolution or the inverse filter. In the case considered here, the reconstructed time series can be represented as the sum of the real parts of the wavelet transforms over all scales [26]:

$$x_n = \frac{\delta j \sqrt{\delta t}}{C \psi_0(0)} \Sigma_{j=0}^{J} \frac{\text{Re}[W_n(s_j)]}{\sqrt{s_j}}. \qquad (22)$$

---

[5]The subscript 0 on ψ has been dropped, in order to indicate that ψ has also been normalized (see later).

The factor $\psi_0(0)$ removes the energy scaling while the $\sqrt{s_j}$ converts the wavelet transform to an energy density. The factor C comes from the reconstruction of a δ function from its wavelet transform using the function $\psi_0(\eta)$ (12) and is a constant for each type of wavelet function. The total energy is conserved by the wavelet transform, and the equivalent of Parseval's theorem for wavelet analyses is

$$\sigma^2 = \frac{\delta j \delta t}{CN} \Sigma_{n=0}^{N-1} \Sigma_{j=0}^{J} \frac{|W_n(s_j)|^2}{s_j}. \quad (23)$$

To determine significance levels for either Fourier or wavelet spectra, one first needs to choose an appropriate background spectrum. It is then assumed that different realizations of the neutrino emission process will be randomly distributed about this mean or expected background, and the actual spectrum is compared with this random distribution. For our phenomena, an appropriate background spectrum could be either white noise (with a flat Fourier spectrum) or red noise (increasing power with decreasing frequency). Here, for simplicity we choose a Gaussian white-noise background spectrum.

We define as follows the null hypothesis for the wavelet power spectrum: we assume that the time series has a mean power spectrum, given simply by $P_k = 1$ in case of the white noise. If a peak in the wavelet power spectrum appears significantly above this background spectrum, then it is considered to be a true feature with a certain percentage confidence. If x_n is a normally distributed random variable, then both the real and imaginary part of $\hat{x}_k$ are normally distributed. Since the square of a normally distributed variable is chi-squared distributed with 1 degree of freedom (DOF), then the $|\hat{x}_k|^2$ variable has a chi-squared distribution with two DOFs, χ_2 [27]. In the case that the original Fourier components are normally distributed, the wavelet coefficients should also be normally distributed, while the wavelet power spectrum $|W_n(s)|^2$ should have a χ_2^2 distribution. Thus, if the background were truly white noise, the distribution shown in the middle panel of Fig. 1 would have a χ_2^2 distribution for each point of (t, s). In summary, assuming a mean background spectrum of white (red) noise form, the distribution of the Fourier power spectrum reads

$$\frac{N|\hat{x}_k|^2}{\sigma^2} \Rightarrow P_k \chi_2^2 \quad (24)$$

at each Fourier frequency index k, with P_k being the mean spectrum value corresponding to the wavelet scale s at this index. (Here, the sign $\Rightarrow$ means "is distributed as.") The corresponding distribution for the local wavelet power spectrum is

$$\frac{|W_n(s)|^2}{\sigma^2} \Rightarrow \frac{1}{2} P_k \chi_2^2 \quad (25)$$

at each time n and scale s. Disregarding the relation between k and s, the relation (25) is independent of the wavelet function. After finding an appropriate background spectrum, simply the white nose in our case, and choosing a particular confidence level for χ^2 such as 95%, one can then use (25) at each scale and build 95% contour lines, as seen in the middle panel of Fig. 1.

In order to examine fluctuations in power over a range of scales (s_1, s_2) (a band), one can define the scale-averaged wavelet power as the weighted sum of the wavelet power spectrum over the scales s_1 to s_2:

$$\bar{W}_n^2 = \frac{\delta j \delta t}{C} \Sigma_{j=j_1}^{j_2} \frac{|W_n(s_j)|^2}{s_j}. \quad (26)$$

The scale-averaged wavelet power can be used to examine modulation of one time series by another, or modulation of one frequency by another within the same time series.

It is convenient to normalize the wavelet power by the expectation value for a white-noise time series. From (26), this expectation value is $(\delta j \delta t \sigma^2)/(CS_{\text{avg}})$, where S_{avg} is defined as

$$S_{\text{avg}} = \left(\Sigma_{j=j_1}^{j_2} \frac{1}{s_j} \right)^{-1}. \quad (27)$$

Using the normalization factor for white noise, the distribution can be modeled in analogy with (25), namely,

$$\frac{CS_{\text{avg}}}{\delta j \delta t \sigma^2} \bar{W}_n^2 \Rightarrow \bar{P} \frac{\chi_\vartheta^2}{\vartheta}, \quad (28)$$

where the scale-averaged theoretical spectrum is now given by

$$\bar{P} = S_{\text{avg}} \Sigma_{j=j_1}^{j_2} \frac{P_j}{s_j}, \quad (29)$$

and χ_ϑ^2 is the chi-squared distribution with the number of DOFs ϑ. Note that for white noise the normalization is such that this spectrum is still unity. The number of DOFs ϑ in (28) is modeled as

$$\vartheta = \frac{2 n_a S_{\text{avg}}}{S_{\text{mid}}} \sqrt{1 + \left(\frac{n_a \delta j}{\delta j_0} \right)^2}, \quad (30)$$

where $S_{\text{mid}} = s_0 2^{0.5(j_1 + j_2)\delta j}$ and $n_a = j_2 - j_1 + 1$. The factor $S_{\text{avg}}/S_{\text{mid}}$ corrects for the loss of DOFs that arises from dividing the wavelet power spectrum by the scale in (26).

III. RESULTS OF THE ANALYSIS

A. Wavelet transforms of the neutrino time series

The neutrino time series found in [5], summing over all the produced neutrino energies, is shown in the top panel of Fig. 1.[6] We see that it exhibits structures on time scales below a hundredth of a second that appear, *prima facie*, to

---

[6]The binning is chosen at the level of a good fraction of ms, which seems to be reasonable for water Čerenkov and scintillator detectors.

be far beyond the magnitude of fluctuations that could be expected from a "featureless" white-noise spectrum. As discussed in the previous section, the wavelet technique is very suitable for extracting such structures, and has been applied in analogous analyses of time structures in photon emissions from gamma-ray bursters [12]. The middle panel of Fig. 1 shows the normalized wavelet power spectrum, $|W_n(s)|^2/\sigma^2$, for the time series of the neutrino emission shown in the top panel. The normalization by $1/\sigma^2$ gives a measure of the power relative to white noise, and the colors represent the significance of the feature compared to a white-noise spectrum. We see that the wavelet transform picks out structures in the time series on time scales down to $\sim 2 \times 10^{-3}$ s. Several of these structures in the time series have high significance, well above the 95% C.L. for a white-noise spectrum (indicated by red contours). These can be seen in the bottom panel of Fig. 1, where stuctures with time scales between 2 and 3 ms are selected. We note, in particular, the series of structures appearing at times between 0.22 and 0.34 s after the start. There are also structures in the band between 7 and 15 ms, and also appreciable power at longer periods. Since we are interested in obtaining the best resolution possible, in the following we focus on the band corresponding to the smallest range of the scales where significant power is seen, namely, that between 2 and 3 ms.[7]

Here, we investigate how these structures would be smeared out by the energy-dependent refractive index or by a stochastic spread in the velocities of different neutrinos with the same energy, the two possibilities described in the previous section. Specifically, we study the following possible energy dependences of the neutrino group velocity $v_{g\nu}$:

$$\frac{v_{g\nu}}{c} = 1 \pm \left(\frac{E}{M_{\nu LV(1/2)}}\right)^{1/2}, \qquad (31)$$

$$\frac{v_{g\nu}}{c} = 1 \pm \frac{E}{M_{\nu LV1}}, \qquad (32)$$

$$\frac{v_{g\nu}}{c} = 1 \pm \left(\frac{E}{M_{\nu LV2}}\right)^2. \qquad (33)$$

We also investigate a possible stochastic effect which may change the arrival times, t, of individual neutrinos, assuming a Gaussian probability distribution function:

---

[7]However, we do note that these would be the most endangered by directional averaging of neutrinos streaming in all directions, as may occur in more complete two-dimensional or three-dimensional treatments of the neutrino transport. In contrast, the time structures connected to the typical SASI and convective time scales (tens of Hertz up to about 200 Hz) are likely to survive even in three dimensions (though possibly with a somewhat reduced amplitude) [7,8]. If the minimum period of neutrino variability were to increase, the sensitivity of our analysis would decrease correspondingly.

$$\mathcal{P}(t^{\text{stoch}}) = \frac{1}{\sigma\sqrt{2\pi}} \exp\left[-\frac{(t^{\text{stoch}} - t)^2}{2\sigma^2}\right], \qquad (34)$$

as discussed above. Here, $\sigma = \gamma_l E^l$ with constants γ_l and $l = 0, 1,$ and 2.

B. Sensitivity to an energy-dependent refractive index for neutrinos

Lower limits on $M_{\nu LV(1/2)}$, $M_{\nu LV1}$, $M_{\nu LV2}$, and γ_l may be calculated by requiring that the fine-scale time structures in the wavelet power spectrum do not disappear below the 95% C.L. of significance for a signal above the white-noise power spectrum. Specifically, for the models (31)–(33) we apply to every neutrino event an energy-dependent time shift

$$\Delta t = \tau_l E^l, \qquad (35)$$

where

$$\tau_l = \frac{L}{cM_{\nu LVl}^l}, \qquad (36)$$

and $l = \frac{1}{2}, 1, 2$. We then vary τ_l ($M_{\nu LVl}$) and follow the evolution of the signal in the neutrino time series. If there is a nontrivial dispersive effect during propagation from the source, it can be compensated by choosing the "correct" value of the time shift τ_l, in which case the original time structure at the source is recovered. On the other hand, dispersion at the source itself could not, in general, be compensated by any choice of τ_l. Quantitatively, the time structure of the supernova signal is recovered by maximizing the fraction of the scale-averaged power spectrum above the 95% C.L. line. In order to calculate a lower limit on τ_l in any specific model, we examine the fine-scale time structures that appear above the 95% C.L. in the bottom panel of Fig. 1 and find the value of the time-shift parameter (36) at which the signal above the 95% C.L. disappears.

We first study a linearly energy-dependent neutrino refractive index of the form $1 + (E/M_{\nu LV1})$. Figure 3 displays the result of one simulation of the effect of such an energy-dependent refractive index, sampled in 21 bins corresponding to different time shifts τ_1. The vertical axis shows the strengths of the emissions in the structures with time scales between 2×10^{-3} s and 3×10^{-3} s, applying a linear energy-dependent time shift $\tau_1 = 4.2 \times 10^{-5}$(s/MeV). Looking at the structures that occur between 0.22 and 0.34 s after the start, we find that the significant portions of these small-scale structures (those that rise above the 95% fluctuation level for white-noise background neutrino emission) disappear for time delays $\tau > 4.20 \times 10^{-5}$(s/MeV), corresponding to $M_{\nu LV1} > 2.45 \times 10^{13}$ GeV if a supernova distance L of 10 kpc is assumed. This sensitivity is 2 orders of magnitude more sensitive than that found in [15], namely $M_{\nu LV1} > 2.2 \times 10^{11}$ GeV, based on a one-dimensional simulation of a
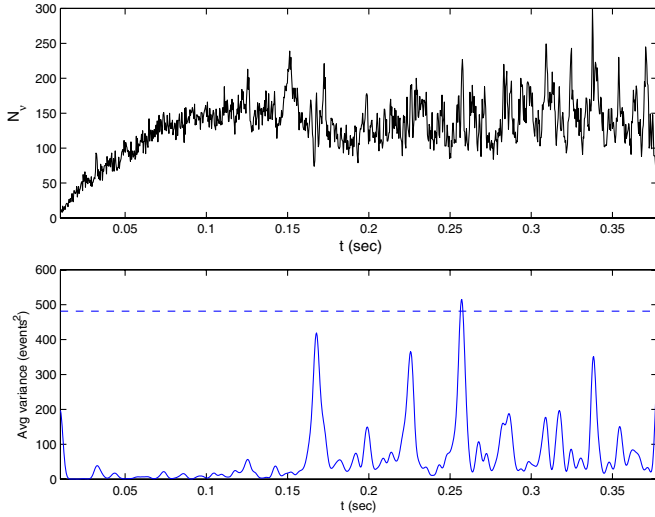
FIG. 3 (color online). The strength of the time-scale structure of the power spectrum averaged between 0.002 and 0.003 s disappears below the 95% C.L. of significance after applying a linear energy-dependent time shift $\tau_1 = 4.2 \times 10^{-5}$(s/MeV).

core-collapse supernova that did not exhibit the small time-scale structures seen in Fig. 1.

We have repeated this exercise with 25 different statistical realizations of the neutrino emission, calculating in each case the amount Σ of the total signal above 95% C.L. for different values of τ_1 sampled in 21 bins. The results of these 25 realizations can be fit quite well by a Gaussian distribution, as seen in Fig. 4. (In this and subsequent figures, we concentrate on the structures with time scales between 2×10^{-3} s and 3×10^{-3} s that occur between 0.22 and 0.34 s after the start.) One can see that the position of the maximum, which defines the value of τ that maximizes the time structures in the signal and is expected to be zero, is indeed consistent with zero to within a
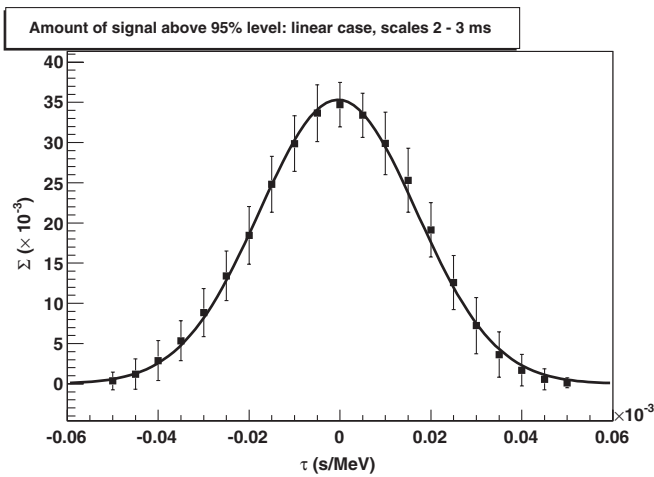
precision of 10^{-6}(s/MeV), while the structures are washed out to below the 1σ level at

$$\tau_1 = 3.85[3.95] \times 10^{-5} \text{ s/MeV}, \qquad (37)$$

where the number in square brackets $[\dots]$ is obtained from a similar analysis of the superluminal case. On the basis of this analysis, if significant time structures of the type found in the two-dimensional simulation [5] were to be seen in IceCube in neutrino data from a core-collapse supernova at a distance of 10 kpc, one could conclude that

$$M_{\nu\text{LV1}} > 2.68[2.61] \times 10^{13} \text{ GeV} \qquad (38)$$

for a neutrino refractive index of the form $1 \pm (E/M_{\nu\text{LV1}})$. On the other hand, if no such structures were seen, inferring an upper limit on $M_{\nu\text{LV1}}$ would require strong independent confirmation of the structures found in [5], in particular, by full three-dimensional simulations.

We have repeated this analysis for the case of a quadratic energy dependence in the refractive index of the form $1 \pm (E/M_{\nu\text{LV2}})^2$, finding the results shown in Fig. 5. In this case, we find that the structures are washed out to below the 1σ level when

$$\tau_2 = 1.10[1.11] \times 10^{-6} \text{ s/MeV}^2, \qquad (39)$$

where the number in square brackets is again obtained from a similar analysis of the superluminal case. Hence, observation of significant time structures [5] in IceCube would imply that

$$M_{\nu\text{LV2}} > 0.97[0.96] \times 10^6 \text{ GeV}, \qquad (40)$$

if such structures were to be observed in a supernova explosion at 10 kpc, again with the proviso that inferring an upper limit on $M_{\nu\text{LV2}}$ would require strong confirmation of the structures found in [5], specifically by full three-dimensional simulations.
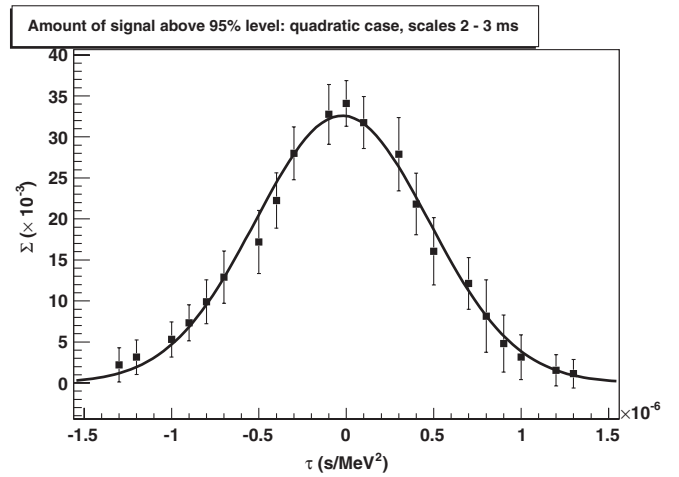

FIG. 4. A Gaussian fit to the amount Σ of the short time-scale signal above the 95% C.L., calculated for 21 values of the shift parameters τ_1. Each point is obtained as the average over 25 realizations of the time-energy assignments of individual neutrinos.
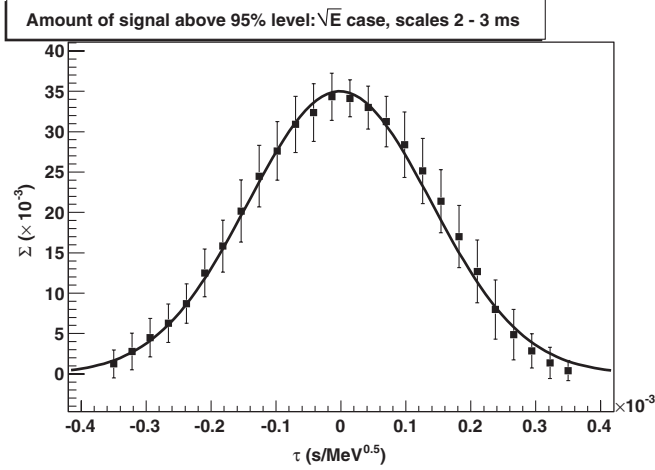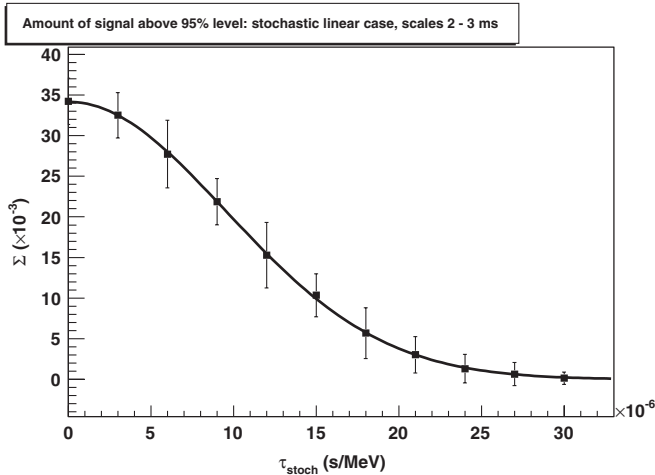

FIG. 5. A Gaussian fit to the amount Σ of the short time-scale signal above the 95% C.L. calculated for 21 values of the shift parameters τ_2. Each point is obtained as the average over 25 realizations of the time-energy assignments of individual neutrinos.
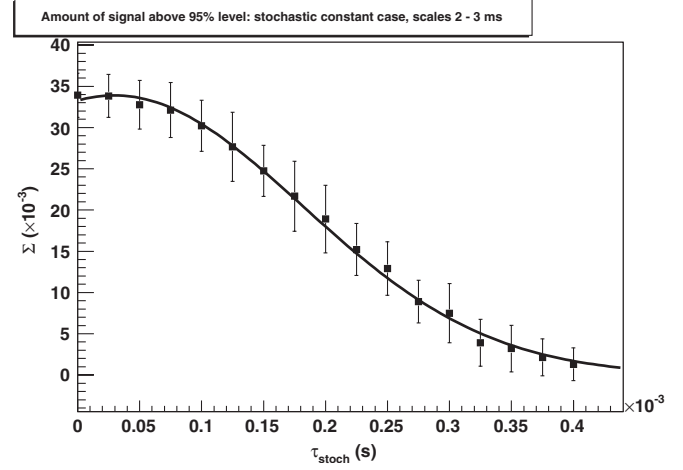
FIG. 6. A Gaussian fit to the amount Σ of the short time-scale signal above the 95% C.L. calculated for 26 values of the shift parameters $\tau_{(1/2)}$. Each point is obtained as the average over 25 realizations of the time-energy assignments of individual neutrinos.

Finally, repeating this analysis for the case $1 \pm \sqrt{E/M_{\nu\mathrm{LV}(1/2)}}$, we find the results shown in Fig. 6:

$$\tau_{1/2} = 3.10[3.15] \times 10^{-4} \text{ s/}\sqrt{\text{MeV}}, \quad (41)$$

(again, square brackets denote the superluminal case) corresponding to a sensitivity to

$$M_{\nu\mathrm{LV}(1/2)} > 1.11[1.07] \times 10^{22} \text{ GeV} \quad (42)$$

if such structures were to be observed in a supernova explosion at 10 kpc.

FIG. 8. A Gaussian fit to the amount Σ of the short time-scale signal above the 95% C.L. calculated for 17 values of the shift parameters τ_0^{stoch}. Each point is obtained as the average over 35 realizations of the time-energy assignments of individual neutrinos.

C. Sensitivity to a stochastic spread in neutrino velocities

The possibility of a stochastic spread in the velocities of individual neutrinos with the same energy can be investigated in a similar way. As discussed in Sec. II, the amount of velocity spread σ might be energy independent, and we consider this possibility as well as possible linear and quadratic energy dependences of σ. As in the case of an energy-dependent time delay, any of these possibilities would tend to spread out and reduce the significances of the peaks found in the wavelet analysis shown in Fig. 1.
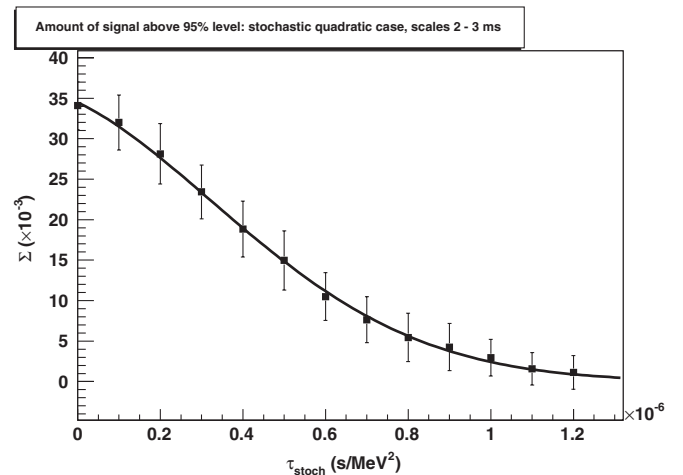

FIG. 7. A Gaussian fit to the amount Σ of the short time-scale signal above the 95% C.L. calculated for 11 values of the shift parameters τ_1^{stoch}. Each point is obtained as the average over 35 realizations of the time-energy assignments of individual neutrinos.

FIG. 9. A Gaussian fit to the amount Σ of the short time-scale signal above the 95% C.L. calculated for 13 values of the shift parameters τ_2^{stoch}. Each point is obtained as the average over 35 realizations of the time-energy assignments of individual neutrinos.

This effect is seen for $\sigma \propto E$ in Fig. 7, for the energy-independent case in Fig. 8, and for $\sigma \propto E^2$ in Fig. 9. In each case, we plot results obtained from 35 independent statistical simulations of the neutrino emission signal. We see that the wavelet peaks are reduced below the 95% C.L. white-noise level for

$$\tau_{\text{stoch1}} = 2.16 \times 10^{-5} \text{ s/MeV} \qquad (43)$$

in the linear case,

$$\tau_{\text{stoch2}} = 9.56 \times 10^{-7} \text{ s/MeV}^2 \qquad (44)$$

in the quadratic case, and

$$\tau_{\text{stoch0}} = 3.59 \times 10^{-4} \text{ s} \qquad (45)$$

in the energy-independent case.[8] These sensitivities correspond to $M_{\nu\text{LV1}} > 4.78 \times 10^{13}$ GeV and $M_{\nu\text{LV2}} > 1.04 \times 10^6$ GeV in the energy-dependent cases, for a supernova explosion at 10 kpc.

IV. CONCLUSIONS AND PROSPECTS

We have shown that the existence of structures with short time scales in the neutrino emission from a core-collapse supernova, as suggested by two-dimensional simulations [5], would open up new possibilities for probing aspects of the propagation of neutrinos that lie far beyond the reach of terrestrial experiments, and up to 2 orders of magnitude beyond the sensitivity provided by previous analyses based on one-dimensional supernova simulations. This increased sensitivity holds for possible square-root, linear and quadratic dependences of the neutrino refractive index, and for both energy-independent and linear or quadratically dependent stochastic spreads in the velocities of different neutrinos with the same energy.

Specifically, if such short time structures are seen in a supernova explosion at a distance of 10 kpc, one could infer that

$$M_{\nu\text{LV}(1/2)} > 1.11[1.07] \times 10^{22} \text{ GeV}, \qquad (46)$$

$$M_{\nu\text{LV1}} > 2.68[2.61] \times 10^{13} \text{ GeV}, \qquad (47)$$

$$M_{\nu\text{LV2}} > 0.97[0.96] \times 10^6 \text{ GeV}, \qquad (48)$$

$$M_{\underset{\nu\text{LV1}}{\sim}} > 4.78 \times 10^{13} \text{ GeV}, \qquad (49)$$

$$M_{\underset{\nu\text{LV2}}{\sim}} > 1.04 \times 10^6 \text{ GeV}, \qquad (50)$$

where the numbers in square brackets correspond to the superluminal case, and the last two limits correspond to the possible effects of stochastic fluctuations. In the case of an energy-independent stochastic spread, one could infer that $\tau_{\text{stoch0}} < 3.59 \times 10^{-4}$ s.

If such short time structures are not seen, many checks would be necessary before one could conceivably claim observation of any unconventional effect in neutrino propagation. In particular, it would be necessary to validate the predictions of the two-dimensional core-collapse supernova simulation on which this analysis is based, specifically by confirming that short time structures are also found in full three-dimensional simulations [7,8]. We hope that the interesting sensitivity to new neutrino physics discussed in this paper—not to mention OPERA [19]—will add to the motivation to develop further such simulations and derive robust predictions for neutrino emissions from core-collapse supernovae.

---

[8]For comparison, we note that the OPERA result [19] also provides an upper limit on the stochastic spread of about 10 ns, though after propagation over a much shorter distance $\sim$730 km. However, using Eqs. (2)–(5) we find that neither OPERA nor SN1987a gives competitive constraints on the scales $M_{\nu\text{LV}l}$.

[1] For a review, see A. Strumia and F. Vissani, arXiv:hep-ph/0606054; for a review of neutrino astronomy, see Y. Totsuka, Rep. Prog. Phys. **55**, 377 (1992).

[2] K. Hirata *et al.* (KAMIOKANDE-II Collaboration), Phys. Rev. Lett. **58**, 1490 (1987); see also E. N. Alekseev, L. N. Alekseeva, V. I. Volchenko, and I. V. Krivosheina, Pis'ma

Zh. Eksp. Teor. Fiz. **45**, 461 (1987) [JETP Lett. **45**, 589 (1987)]; E. N. Alekseev, L. N. Alekseeva, I. V. Krivosheina, and V. I. Volchenko, Phys. Lett. B **205**, 209 (1988).

[3] R. Buras, H.-T. Janka, M. Rampp, and K. Kifonidis, Astron. Astrophys. **457**, 281 (2006); A. Marek and H.-T. Janka, Astrophys. J. **694**, 664 (2009); R. Walder, A. Burrows, C. D. Ott, E. Livne, I. Lichtenstadt, and M. Jarrah, Astrophys. J. **626**, 317 (2005); Y. Suwa, K. Kotake, T. Takiwaki, S. C. Whitehouse, M. Liebendörfer, and K. Sato, Publ. Astron. Soc. Jpn. **62**, L49 (2010) [http://pasj.asj.or.jp/v62/n6/620601/620601a.html]; K. Yakunin, P. Marronetti, A. Mezzacappa, S. W. Bruenn, C.-T. Lee, M. A. Chertkow, W. R. Hix, J. M. Blondin, E. J. Lentz, B. O. E. Messer, and S. Yoshida, Classical Quantum Gravity **27**, 194005 (2010).

[4] C. D. Ott, A. Burrows, L. Dessart, and E. Livne, Astrophys. J. **685**, 1069 (2008); T. D. Brandt, A. Burrows, C. D. Ott, and E. Livne, Astrophys. J. **728**, 8 (2011).

[5] A. Marek, H.-T. Janka, and E. Müller, Astron. Astrophys. **496**, 475 (2009); T. Lund, A. Marek, C. Lunardini, H.-T. Janka, and G. Raffelt, Phys. Rev. D **82**, 063007 (2010).

[6] P. Desiati (IceCube Collaboration), arXiv:1007.2621, and references therein.

[7] S. W. Bruenn, A. Mezzacappa, W. R. Hix, J. M. Blondin, P. Marronetti, O. E. B. Messer, C. J. Dirk, and S. Yoshida, J. Phys. Conf. Ser. **180**, 012018 (2009); T. Takiwaki, K. Kotake, and Y. Suwa, arXiv:1108.3989 [Astrophys. J. (to be published)].

[8] E. Müller, H.-T. Janka, and A. Wongwathanarat, Astron. Astrophys. **537**, A63 (2012).

[9] W. D. Arnett and J. L. Rosner, Phys. Rev. Lett. **58**, 1906 (1987); E. W. Kolb, A. J. Stebbins, and M. S. Turner, Phys. Rev. D **35**, 3598 (1987); G. G. Raffelt, *Stars as Laboratories for Fundamental Physics* (University of Chicago, Chicago, 1996).

[10] G. Amelino-Camelia, J. R. Ellis, N. E. Mavromatos, and D. V. Nanopoulos, Int. J. Mod. Phys. A **12**, 607 (1997); J. R. Ellis, N. E. Mavromatos, and D. V. Nanopoulos, Phys. Lett. B **293**, 37 (1992); *Erice Subnucl. Phys. Series*, (World Scientific, Singapore, 1994), Vol. 31, p. 1; Chaos Solitons Fractals **10**, 345 (1999); G. Amelino-Camelia, arXiv:0806.0339, and references therein.

[11] G. Amelino-Camelia, J. Ellis, N. Mavromatos, D. Nanopoulos, and S. Sarkar, Nature (London) **393**, 763 (1998).

[12] J. R. Ellis, N. E. Mavromatos, D. V. Nanopoulos, and A. S. Sakharov, Astron. Astrophys. **402**, 409 (2003); J. R. Ellis, N. E. Mavromatos, D. V. Nanopoulos, A. S. Sakharov, and E. K. G. Sarkisyan, Astropart. Phys. **25**, 402 (2006); **29**, 158 (2008).

[13] R. Gambini and J. Pullin, Phys. Rev. D **59**, 124021 (1999); J. Alfaro, H. A. Morales-Tecotl, and L. F. Urrutia, Phys. Rev. D **65**, 103509 (2002); V. A.

[14] J. R. Ellis, N. E. Mavromatos, and D. V. Nanopoulos, Phys. Lett. B **665**, 412 (2008); T. Li, N. E. Mavromatos, D. V. Nanopoulos, and D. Xie, Phys. Lett. B **679**, 407 (2009); N. E. Mavromatos, Int. J. Mod. Phys. A **25**, 5409 (2010).

[15] J. R. Ellis, N. Harries, A. Meregaglia, A. Rubbia, and A. Sakharov, Phys. Rev. D **78**, 033013 (2008).

[16] J. R. Ellis, N. E. Mavromatos, and D. V. Nanopoulos, Gen. Relativ. Gravit. **32**, 127 (2000); J. R. Ellis, K. Farakos, N. E. Mavromatos, V. A. Mitsou, and D. V. Nanopoulos, Astrophys. J. **535**, 139 (2000).

[17] N. E. Mavromatos, Lect. Notes Phys. **669**, 245 (2005); D. Hooper, D. Morgan, and E. Winstanley, Phys. Lett. B **609**, 206 (2005); D. Morgan, E. Winstanley, J. Brunner, and L. F. Thompson, Astropart. Phys. **25**, 311 (2006); G. Barenboim, N. E. Mavromatos, S. Sarkar, and A. Waldron-Lauda, Nucl. Phys. **B758**, 90 (2006); N. E. Mavromatos, A. Meregaglia, A. Rubbia, A. Sakharov, and S. Sarkar, Phys. Rev. D **77**, 053014 (2008).

[18] P. Adamson *et al.* (MINOS Collaboration), Phys. Rev. D **76**, 072005 (2007); see also G. R. Kalbfleisch, N. Baggett, E. C. Fowler, and J. Alspector, Phys. Rev. Lett. **43**, 1361 (1979).

[19] T. Adam *et al.* (OPERA Collaboration), arXiv:1109.4897.

[20] J. Alexandre, J. Ellis, and N. E. Mavromatos, Phys. Lett. B **706**, 456 (2012); see also G. Cacciapaglia, A. Deandrea, and L. Panizzi, J. High Energy Phys. 11 (2011) 137; G. F. Giudice, S. Sibiryakov, and A. Strumia, arXiv:1109.5682; L. Maccione, S. Liberati, and D. M. Mattingly, arXiv:1110.0783.

[21] See, for instance, R. Lehnert and R. Potting, Phys. Rev. D **70**, 125010 (2004); B. Altschul, Phys. Rev. Lett. **98**, 041603 (2007), and references therein.

[22] J. M. Lattimer and F. D. Swesty, Nucl. Phys. **A535**, 331 (1991).

[23] J. M. Blondin, A. Mezzacappa, and C. DeMarino, Astrophys. J. **584**, 971 (2003); L. Scheck, H. T. Janka, T. Foglizzo, and K. Kifonidis, Astron. Astrophys. **477**, 931 (2008).

[24] J. M. Blondin and A. Mezzacappa, Nature (London) **445**, 58 (2007); T. Yamasaki and T. Foglizzo, Astrophys. J. **679**, 607 (2008); R. Fernández, Astrophys. J. **725**, 1563 (2010).

[25] S. A. Mallat, *Wavelet Tour of Signal Processing* (Academic, San Diego, 1998).

[26] C. Torrence and G. P. Compo, Bull. Am. Meteorol. Soc. **79**, 61 (1998); M. Farge, Annu. Rev. Fluid Mech. **24**, 395 (1992).

[27] G. M. Jenkins and D. G. Watts, *Spectral Analysis and Its Applications* (Emerson Adams Press Inc., Boca Raton, Fl, 1998).